

On relation between Parton Branching Approach and CCFM evolution

A.V. Lipatov^{1,2}, M.A. Malyshev^{1*}, H. Jung³

October 25, 2019

¹*Skobeltsyn Institute of Nuclear Physics, Lomonosov Moscow State University, 119991 Moscow, Russia*

²*Joint Institute for Nuclear Research, Dubna 141980, Moscow Region, Russia*

³*Deutsches Elektronen-Synchrotron, 22603 Hamburg, Germany*

Abstract

We consider the associated production of electroweak gauge bosons and charm or beauty quark jets at the LHC using the k_T -factorization framework. We apply the transverse momentum dependent (TMD) parton distributions in a proton obtained from the Parton Branching (PB) method as well as from the Catani-Ciafaloni-Fiorani-Marchesini (CCFM) evolution equation. For the PB approach, our prescription merges the standard leading order $\mathcal{O}(\alpha\alpha_s)$ k_T -factorization calculations with several tree-level next-to-leading order $\mathcal{O}(\alpha\alpha_s^2)$ off-shell production amplitudes. For the CCFM scenario, our consideration is based on the $\mathcal{O}(\alpha\alpha_s^2)$ off-shell gluon-gluon fusion subprocess $g^*g^* \rightarrow Z/W + Q\bar{Q}$ and some subleading $\mathcal{O}(\alpha\alpha_s^2)$ subprocesses involving quark interactions, taken into account in conventional (collinear) QCD factorization. We find that the $W + c$ and $Z + b$ cross sections, calculated within the PB and CCFM-based schemes with the proper choice of leading and next-to-leading subprocesses, are in good agreement with each other, thus establishing a correspondence between these two scenarios. A comparison with the latest LHC experimental data is given and the necessity for the proper off-shell treatment of the production amplitudes in determination of the parameters of the TMD parton density is demonstrated.

PACS number(s): 12.38.-t, 12.38.Bx, 13.85.Qk, 14.65.-q, 14.70.Hp

*e-mail: malyshev@theory.sinp.msu.ru

1 Motivation

A theoretical description of a number of processes at high energies and large momentum transfer containing multiple hard scales requires so-called transverse momentum dependent (TMD, or unintegrated) parton (quark and gluon) density functions [1]. These quantities encode the non-perturbative information on proton structure, including transverse momentum and polarization degrees of freedom and are related to the physical cross sections via different TMD factorization scenarios. The latter provide the necessary framework to separate hard partonic physics, described with a perturbative QCD expansion, from soft hadronic physics.

In the limit of a fixed hard scale and high energy the k_T -factorization [2] (or high-energy factorization [3]) approach is expected to be valid. This approach is mainly based on the Balitsky-Fadin-Kuraev-Lipatov (BFKL) [4] or Ciafaloni-Catani-Fiorani-Marchesini (CCFM) [5] evolution equations for the TMD gluon densities in a proton. The BFKL equation resums large logarithmic terms proportional to $\alpha_s^n \ln^n s \sim \alpha_s^n \ln^n 1/x$, important at high energies s (or, equivalently, at small x). The CCFM equation takes into account additional terms proportional to $\alpha_s^n \ln^n 1/(1-x)$ and is valid at both low and large x . There are also scenarios to evaluate the TMD parton densities based on the conventional Dokshitzer-Gribov-Lipatov-Altarelli-Parisi (DGLAP) [6] evolution equations, namely the Kimber-Martin-Ryskin (KMR) prescription [7] and recently proposed Parton Branching (PB) approach [8, 9]. The KMR approach, currently explored [10] at next-to-leading order (NLO), is a formalism to construct the TMD parton densities from well-known conventional (collinear) ones under the key assumption that the transverse momentum dependence of the parton distributions enters only at the last evolution step. The PB approach provides an iterative solution of the DGLAP evolution equations for collinear and TMD parton density functions by making use of the concept of resolvable and non-resolvable branchings and by applying Sudakov form factors to describe the parton evolution from one scale to another without resolvable branching. The splitting kinematics at each branching vertex is described by the DGLAP equations and angular ordering conditions for parton emissions can be applied here instead of usual DGLAP ordering in virtuality. One of the main advantages of the PB approach is that the TMD parton densities (and all corresponding non-perturbative parameters) can be fitted to experimental data, so that the theoretical predictions, where the parton shower effects are already taken into account, can be obtained with no further free parameters¹.

A number of phenomenological applications of the CCFM evolution equation is known in the literature (see, for example, [11–17] and references therein). Several applications of the PB approach were discussed [18, 19] and comparison between the PB and KMR predictions has been recently made [20, 21]. However, the correspondence between the CCFM and PB scenarios has been not investigated yet. One of the main goals of this paper is to compare predictions for some QCD processes with the CCFM and PB parton distributions, to find a correspondence between these approaches and to define conditions, at which such correspondence takes place. As the reference processes for the study, we consider here the associated production of electroweak gauge bosons (W and Z) and charm or beauty quark jets at the LHC conditions. These are the so-called “rare” processes which could have never been systematically studied at previous accelerators. We already successfully applied [16] the CCFM-evolved gluon densities to describe first LHC data [22, 23] of the associated $Z + b$ production at $\sqrt{s} = 7$ TeV. Those calculations were based on the $\mathcal{O}(\alpha_s^2)$ off-shell gluon-gluon fusion subprocess $g^*g^* \rightarrow Z + Q\bar{Q}$ (where the Z boson further decays into a lepton pair) and several subleading $\mathcal{O}(\alpha_s^2)$ and $\mathcal{O}(\alpha_s^3)$

¹In contrast to the usual parton shower event generators.

subprocesses involving quark-antiquark and quark-gluon interactions, taken into account within the conventional (collinear) QCD factorization. Such a scheme allows us to describe LHC experimental data in the whole transverse momentum range. Here we extend the consideration to associated $W + c$ production, measured [24] by the CMS Collaboration for the first time as a function of W decay lepton and/or c -jet rapidities at $\sqrt{s} = 13$ TeV. Thus, in this sense we continue the line of our previous studies [16]. In contrast to the CCFM scenario, in the PB calculations (as being the DGLAP-based ones) one has to include usual leading order (LO) $\mathcal{O}(\alpha\alpha_s)$ subprocesses properly matched with a number of additional higher-order terms. Below we perform such calculations and matching procedure following the approach applied recently [20] for c -jet production at the LHC. The comparison between the results obtained within the TMD approaches above could be also a general consistency check for the k_T -factorization phenomenology.

The outline of the paper is the following. In Section 2 we briefly discuss the CCFM equation and PB approach and describe the basic steps of our calculations. In Section 3 we present the results of our calculations and discussion. Our conclusions are summarised in Section 4.

2 Theoretical framework

2.1 CCFM evolution

The CCFM gluon evolution equation resums large logarithms $\alpha_s^n \ln^n 1/(1-x)$ in addition to BFKL ones $\alpha_s^n \ln^n 1/x$ and introduces angular ordering of initial emissions to correctly treat gluon coherence effects. In the limit of asymptotic energies, it is almost equivalent to BFKL, but also similar to the DGLAP evolution for large x [5]. In the leading logarithmic approximation, the CCFM equation for TMD gluon density $\mathcal{A}(x, \mathbf{k}_T^2, \mu^2)$ with respect to the evolution (factorization) scale μ^2 can be written as

$$\begin{aligned} \mathcal{A}(x, \mathbf{k}_T^2, \mu^2) = & \mathcal{A}^{(0)}(x, \mathbf{k}_T^2, \mu_0^2) \Delta_s(\mu, \mu_0) + \\ & + \int \frac{dz}{z} \int \frac{dq^2}{q^2} \Theta(\mu - zq) \Delta_s(\mu, zq) \tilde{P}_{gg}(z, \mathbf{k}_T^2, q^2) \mathcal{A}\left(\frac{x}{z}, \mathbf{k}_T^2, q^2\right), \end{aligned} \quad (1)$$

where $\mathbf{k}'_T = \mathbf{q}(1-z) + \mathbf{k}_T$ and $\tilde{P}_{gg}(z, \mathbf{k}_T^2, q^2)$ is the CCFM splitting function:

$$\begin{aligned} \tilde{P}_{gg}(z, \mathbf{k}_T^2, q^2) = & \bar{\alpha}_s(q^2(1-z)^2) \left[\frac{1}{1-z} + \frac{z(1-z)}{2} \right] + \\ & + \bar{\alpha}_s(\mathbf{k}_T^2) \left[\frac{1}{z} - 1 + \frac{z(1-z)}{2} \right] \Delta_{ns}(z, \mathbf{k}_T^2, q^2). \end{aligned} \quad (2)$$

The Sudakov and non-Sudakov form factors read:

$$\ln \Delta_s(\mu, \mu_0) = - \int_{\mu_0^2}^{\mu^2} \frac{d\mu'^2}{\mu'^2} \int_0^{z_M=1-\mu_0/\mu'} dz \frac{\bar{\alpha}_s(\mu'^2(1-z)^2)}{1-z}, \quad (3)$$

$$\ln \Delta_{ns}(z, \mathbf{k}_T^2, \mathbf{q}_T^2) = -\bar{\alpha}_s(\mathbf{k}_T^2) \int_0^1 \frac{dz'}{z'} \int \frac{dq^2}{q^2} \Theta(\mathbf{k}_T^2 - q^2) \Theta(q^2 - z'^2 \mathbf{q}_T^2). \quad (4)$$

where $\bar{\alpha}_s = 3\alpha_s/\pi$. The first term in the CCFM equation, which is the initial TMD gluon density multiplied by the Sudakov form factor, corresponds to the contribution of

non-resolvable branchings between the starting scale μ_0^2 and scale μ^2 . The second term describes the details of the QCD evolution expressed by the convolution of the CCFM gluon splitting function with the gluon density and the Sudakov form factor. The theta function introduces the angular ordering condition. The evolution scale μ^2 is defined by the maximum allowed angle for any gluon emission [5]. A similar equation also can be written [26] for valence quark densities² (with replacement of the gluon splitting function by the quark one). Usually, the initial TMD gluon and valence quark distributions are taken as

$$x\mathcal{A}_g^{(0)}(x, \mathbf{k}_T^2, \mu_0^2) = Nx^{-B}(1-x)^C \exp(-\mathbf{k}_T^2/\sigma^2), \quad (5)$$

$$x\mathcal{A}_{qv}^{(0)}(x, \mathbf{k}_T^2, \mu_0^2) = xq_v(x, \mu_0^2) \exp(-\mathbf{k}_T^2/\sigma^2)/\sigma^2, \quad (6)$$

where $\sigma = \mu_0/\sqrt{2}$ and $q_v(x, \mu^2)$ is the standard (collinear) density function. The parameters of the initial TMD parton distributions can be fitted from the collider data (see, for example, [26, 28]).

The CCFM equation can be solved numerically using the UPDFEVOLV program [29], and the TMD gluon and valence quark densities can be obtained for any x , \mathbf{k}_T^2 and μ^2 values. The main advantage of this approach is the ease of including higher-order radiative corrections (namely, a part of NLO + NNLO +... terms corresponding to the initial-state real gluon emissions) even within LO. More details can be found, for example, in review [1].

2.2 Parton Branching approach

The Parton Branching approach was introduced [8, 9] to treat the DGLAP evolution. The method provides an iterative solution of the evolution equations and agrees with the usual methods to solve the DGLAP equations for inclusive distributions at the NLO and NNLO. It allows one to take into account simultaneously soft-gluon emission at $z \rightarrow 1$ and transverse momentum \mathbf{q}_T recoils in the parton branchings along the QCD cascade. The latter leads to a natural determination of the TMD quark and gluon densities. A soft-gluon resolution scale z_M is introduced to separate resolvable and non-resolvable emissions, which are treated via the DGLAP splitting functions $P_{ab}(\alpha_s, z)$ and Sudakov form-factors, respectively. The PB equations for TMD parton densities read:

$$\begin{aligned} x\mathcal{A}_a(x, \mathbf{k}_T^2, \mu^2) = & x\mathcal{A}_a^{(0)}(x, \mathbf{k}_T^2, \mu_0^2)\Delta_a(z_M, \mu, \mu_0) + \\ & + \sum_b \int_x^{z_M} dz \int \frac{dq^2}{q^2} \Theta(\mu^2 - q^2) \Theta(q^2 - \mu_0^2) \Delta_a(z_M, \mu, q) P_{ab}(\alpha_s, z) \frac{x}{z} \mathcal{A}_b\left(\frac{x}{z}, \mathbf{k}_T'^2, q^2\right), \end{aligned} \quad (7)$$

where $\mathbf{k}_T' = \mathbf{q}(1-z) + \mathbf{k}_T$. The Sudakov form factors are defined as

$$\ln \Delta_a(z_M, \mu, \mu_0) = - \sum_b \int_{\mu_0^2}^{\mu^2} \frac{d\mu'^2}{\mu'^2} \int_0^{z_M} dz z P_{ba}(\alpha_s(\mu'^2), z). \quad (8)$$

The evolution scale μ^2 can be connected with the angle of emitted parton with respect to the beam direction, that leads to the well-known angular ordering condition, $\mu = |\mathbf{q}_T|/(1-z)$. The dependence on the z_M falls out when this angular ordering condition is applied and z_M is large enough. The initial TMD parton distributions are taken in a

²The sea quark distributions are not defined in CCFM. However, they can be obtained from the gluon ones in the last gluon splitting approximation, see [27].

factorized form as a product of collinear quark and gluon densities and intrinsic transverse momentum distributions (treated as gaussian ones [8, 9]), where all the parameters can be fitted from the collider data. Unlike the CCFM parton distributions, the PB densities have the strong normalization property:

$$\int \mathcal{A}_a(x, \mathbf{k}_T^2, \mu^2) d\mathbf{k}_T^2 = f_a(x, \mu^2). \quad (9)$$

The PB evolution equations can be solved by an iterative Monte-Carlo method, that results in a steep drop of the parton densities at $\mathbf{k}_T^2 > \mu^2$. It contrasts the CCFM evolution, where the transverse momentum is allowed to be larger than the scale μ^2 , corresponding to an effective taking into account higher-order contributions³.

2.3 Associated $W^\pm/Z + Q$ production with TMD factorization

To calculate total and differential cross sections of associated gauge bosons and heavy quark jet production within the CCFM-based approach, we strictly follow the scheme [16]. In this scheme, the leading contribution comes from the $\mathcal{O}(\alpha\alpha_s^2)$ off-shell gluon-gluon fusion subprocess

$$g^* + g^* \rightarrow Z + b + \bar{b}, \quad (10)$$

$$g^* + g^* \rightarrow W^- + c + \bar{s}. \quad (11)$$

In addition to off-shell gluon-gluon fusion, one can take into account several $\mathcal{O}(\alpha\alpha_s^2)$ subprocesses involving quarks in the initial state:

$$q + \bar{q} \rightarrow Z + b + \bar{b}, \quad (12)$$

$$q + b \rightarrow Z + b + q, \quad (13)$$

$$g + b \rightarrow Z + b + g \quad (14)$$

for $Z + b$ production and

$$q + \bar{q} \rightarrow W^- + c + \bar{s}, \quad (15)$$

$$q + s \rightarrow W^- + c + q, \quad (16)$$

$$g + s \rightarrow W^- + c + g \quad (17)$$

for $W^- + c$ production. Subprocesses for $W^+ + \bar{c}$ production can be obtained via charge conjugation⁴. The quark-induced diagrams may become important at very large transverse momenta (or, respectively, at large x , which is needed to produce large p_T events) where the quarks are less suppressed or can even dominate over the gluon density. Following [16], the contributions from subprocesses (12), (13), (15) and (16), are taken into account using the collinear DGLAP-based factorization scheme, which provides better theoretical grounds in the large x region⁵. So, we consider a combination of two techniques with each of them being used at the kinematic conditions where it is best suitable. We note that the contributions from the off-shell $\mathcal{O}(\alpha\alpha_s)$ subprocesses, namely,

$$b^* + g^* \rightarrow Z + b, \quad (18)$$

$$s^* + g^* \rightarrow W^- + c \quad (19)$$

³Very recently, a method to incorporate CCFM effects into the PB formulation was proposed [30].

⁴The event selection in [24] is organized in a way to exclude subprocesses with gluon splitting $g \rightarrow c\bar{c}$, so such subprocesses are left out of the consideration.

⁵Subprocesses (14) and (17) are partly taken into account with the gluon fusion subprocesses (10) and (11), respectively, in the k_T -factorization approach.

in the CCFM scheme are covered by gluon-fusion subprocesses (10) or (11) and therefore not taken into account to avoid the double counting. In contrast, in the DGLAP-based PB approach one has to take into account the off-shell $\mathcal{O}(\alpha\alpha_s)$ subprocesses (18) or (19) and properly match them with the higher-order contributions (12) — (14) or (15) — (17), respectively. The details of the matching procedure are discussed below (see Sec. 3.1).

According to k_T -factorization prescription, to calculate the cross sections of processes under consideration we have to convolute the relevant partonic cross sections (related with the off-shell production amplitudes) and TMD parton densities in a proton:

$$\sigma = \sum_{a,b} \int dx_1 dx_2 d\mathbf{k}_{1T}^2 d\mathbf{k}_{2T}^2 d\hat{\sigma}_{ab}^*(x_1, x_2, \mathbf{k}_{1T}^2, \mathbf{k}_{2T}^2, \mu^2) \mathcal{A}_a(x_1, \mathbf{k}_{1T}^2, \mu^2) \mathcal{A}_b(x_2, \mathbf{k}_{2T}^2, \mu^2), \quad (20)$$

where x_1 and x_2 are the longitudinal momentum fractions of the initial off-shell partons and \mathbf{k}_{1T}^2 and \mathbf{k}_{2T}^2 are their transverse momenta. The gauge-invariant off-shell production amplitudes for gluon-gluon fusion subprocesses (10) and (11) were calculated earlier [31, 32] and implemented into the Monte-Carlo event generator CASCADE [33] and newly developed parton-level Monte-Carlo event generator PEGASUS [34]. The off-shell amplitudes for quark induced subprocesses (12) — (14) and (15) — (17) can be derived in the framework of the reggeized parton approach [35]. One can also use Britto-Cachazo-Feng-Witten (BCFW) recursion for off-shell gluons [36] and method of auxilliary quarks for off-shell quarks [37], implemented in the Monte-Carlo generator KATIE [38]. In this study, to calculate the contributions from (12) — (14) and (15) — (17) subprocesses in the PB scheme we used the KATIE tool.

In the present paper we compare the CCFM and PB results obtained with JH'2013 set 1 [26] and PB-NLO-HERAI+II-2018 set 2 [19] TMD parton densities in a proton⁶. The main motivation for our choice is that the input parameters of both these distributions were obtained in exactly the same way: from the best description of precision DIS data on the proton structure functions F_2 with exactly the same angular ordering conditions (see [19, 26] for more information). For the conventional quark and gluon densities we use the MMHT'2014 (LO) set [40].

3 Numerical results

Before we show the results of our calculations, we list the input parameters. We use two-loop running strong coupling formula with $n_f = 5$ massless quark flavours and take $\Lambda_{\text{QCD}} = 200$ MeV in CCFM case and $\Lambda_{\text{QCD}} = 118$ MeV for PB distributions [19, 26]. The QED running coupling is applied with $\alpha(m_Z^2) = 1/128$. The electroweak bosons masses were taken as $m_W = 80.385$ GeV and $m_Z = 91.188$ GeV [41]. As it is often done, we keep the factorization and renormalization scales to be equal to the gauge boson mass. However, in the CCFM scheme we use a different value for factorization scale $\mu_F^2 = \hat{s} + \mathbf{Q}_T^2$, where \hat{s} and \mathbf{Q}_T are the energy of the scattering subprocess and transverse momentum of the incoming off-shell gluon pair. The definition of μ_F is unusual and dictated by the CCFM evolution algorithm [26].

⁶A comprehensive collection of the available TMD parton densities can be found in the TMDLIB package [39].

3.1 Matching $\mathcal{O}(\alpha\alpha_s)$ and $\mathcal{O}(\alpha\alpha_s^2)$ terms in the PB approach

As it was already mentioned above, we supplemented the LO contributions (18) or (19) with off-shell partons in the PB calculations by the tree-level $\mathcal{O}(\alpha_s^2)$ corrections (13) and (14) or (16) and (17) from the emission of one additional parton. However, as it is well known, a problem of possible double counting can occur when mixing different final states. Let us consider the $Z + b$ production (of course, the same arguments apply for $W + c$ case). Here, the off-shell subprocess (18) partially includes contributions from (13) and (14) due to initial state parton radiation, that can result in substantial double counting if these contributions are summed up. To avoid this double counting we limit the integration over the transverse momenta of the incoming off-shell quark and gluon in the factorization formula (20) for the LO subprocess (18) from above with some value k_T^{cut} , so $|\mathbf{k}_{T1}| < k_T^{\text{cut}}$ and $|\mathbf{k}_{T2}| < k_T^{\text{cut}}$. Thus, one removes jets, originating from the initial state radiation and being harder than the initial partons. The latter, however, could be covered by the subprocesses (13) and (14), if we choose there only the events with final gluons and light quarks, having transverse momenta p_T larger, than the cut scale k_T^{cut} . In this way, therefore, we can almost avoid the double counting region.

Of course, the value of k_T^{cut} is not universal but is depending on the process. In order to determine k_T^{cut} we have calculated the differential cross sections of the LO subprocesses (18) or (19) as a function of initial gluon transverse momentum and differential cross sections of the $\mathcal{O}(\alpha_s^2)$ subprocesses (13) or (14) as a function of the produced gluon transverse momentum p_T , see Fig. 1. These calculations were performed in the fiducial kinematical region covered by the ATLAS [23] and CMS [24] experiments (see below). So, fixing the k_T^{cut} at some value would mean that we keep the contribution from the $\mathcal{O}(\alpha_s)$ subprocesses lying to the left from the vertical line with $k_T = k_T^{\text{cut}}$ and complement it with the contribution from the $\mathcal{O}(\alpha_s^2)$ subprocesses right to the vertical line. The resulting matched p_T distribution will have a step-like discontinuous behaviour at $k_T = k_T^{\text{cut}}$. A reasonable choice for the k_T^{cut} would be then the one, with the step being small. We find, that this can be achieved with $k_T^{\text{cut}} \simeq 30$ GeV for associated $Z + b$ -jet production and $k_T^{\text{cut}} \simeq 15$ GeV for $W + c$ -jet production. As one can see from Fig. 1, this choice will lead to the continuous merged transverse momentum distributions.

To investigate the dependence of PB predictions on the k_T^{cut} value in more details we calculated the ratios of fiducial cross sections $\sigma_{\text{PB}}(Z + b)/\sigma_{\text{CCFM}}(Z + b)$ and $\sigma_{\text{PB}}(W + c)/\sigma_{\text{CCFM}}(W + c)$ as a function of k_T^{cut} (note that the denominators in these ratios do not depend on the k_T^{cut}). Our results are shown in Fig. 2. We find that the matched PB predictions are rather stable with variation in k_T^{cut} : both the $Z + b$ -jet and $W + c$ -jet cross sections change less than 5% if $k_T^{\text{cut}} \geq 10$ GeV or $k_T^{\text{cut}} \geq 20$ GeV, respectively. The dependence on k_T^{cut} is smaller than the scale uncertainties of our calculations (see estimation below), so we employ the matching value $k_T^{\text{cut}} = 30$ GeV for $Z + b$ calculations and $k_T^{\text{cut}} = 15$ GeV for $W + c$ production in our numerical calculations.

One can see that with the appropriate choice of k_T^{cut} , as discussed above, the fiducial cross sections calculated in the PB approach are very close to the ones, obtained in the CCFM scheme. The correspondence between these approaches is investigated in detail in the next Section.

3.2 Comparison with the LHC data

We are now in a position to present the results of our simulations and to confront them with the latest LHC data.

The measurements of the associated production of Z bosons and beauty jets have been carried out by the ATLAS [22] and CMS [23] Collaborations and refer to the following categories: Z bosons produced in association with one beauty jet, Z bosons produced in association with two beauty jets, Z bosons associated with any number of b -jets and Z bosons produced in association with explicitly reconstructed b -hadrons. The data on the associated production of W bosons and one charmed jet were reported by the CMS Collaboration very recently for the first time [24]. In the present study we concentrate on the production of gauge bosons associated with one heavy quark jet.

The ATLAS Collaboration has collected the data on $Z+b$ -jet production at the center-of-mass energy $\sqrt{s} = 7$ TeV [22]. Both leptons originating from the Z boson decay are required to have $p_T^l > 20$ GeV and $|\eta^l| < 2.4$, the lepton pair invariant mass lies in the interval $76 < M^{\mu} < 106$ GeV, the beauty jets are required to have $p_T^b > 20$ GeV and $|\eta^b| < 2.4$. The measurement of $W+c$ -jet production at LHC was made by the CMS Collaboration [24] at $\sqrt{s} = 13$ TeV and the fiducial region was defined with the following cuts: the transverse momentum of the c -quark $p_T^c > 5$ GeV, transverse momentum and pseudo-rapidity of the muon originating from W decay should be $p_T^\mu > 26$ GeV and $|\eta^\mu| < 2.4$. The transverse mass of the W boson should be $m_T > 50$ GeV.

We start from $Z+b$ production. In Fig. 3 we present the predictions for the Z boson rapidity and transverse momentum distributions in comparison with the ATLAS [22] data. The solid and dashed histograms corresponds to the results obtained with the JH'2013 set 1 and PB-NLO-HERAI+II-2018 set 2 parton densities. The shaded band represents the scale uncertainties of our PB-based calculations, which have been estimated by varying the scales μ_R and μ_F by a factor of 2 around their default values ⁷. For comparison, we also show the conventional (collinear) NLO pQCD predictions, taken from [22], calculated with MCFM generator [42]. One can see that the Z boson rapidity distribution show almost perfect agreement between the CCFM and PB approaches, demonstrating the consistency between the CCFM and PB approaches. The cross sections are lower, than the ones, obtained in the collinear approach. However, the k_T -factorization based calculations are in better agreement with the data, though slightly overestimating the ATLAS data in the central region. This overestimation is, however, covered by the uncertainties of our calculations. More information can be obtained with the p_T^Z -distributions. The CCFM and PB-based calculations give almost the same very good description of the ATLAS data at small p_T^Z , while at $p_T^Z \gtrsim 100$ GeV the PB-based cross section lies significantly higher, than the CCFM one, and is in better agreement with the data. The reason for that is a more accurate treatment of quark-initiated subprocesses in the PB approach, including also contributions from subprocesses (14) and (17). We would like to note, that both approaches describe the ATLAS data generally better, than the NLO collinear factorization results, especially at low p_T^Z . The scale uncertainties, estimated for PB scheme, are even less, than the ones of collinear NLO predictions.

Now we turn to the $W+c$ -jet production. Our results are shown in Fig. 4, where we plot the decay muon rapidity distributions for both $W^+ + \bar{c}$ and $W^- + c$ events measured by the CMS Collaboration [24]. As in the $Z+b$ production, one can see, that the results, obtained with the CCFM and PB approaches agree very well with each other. This confirms once again the consistency between these approaches. However, our predictions are lower, than the collinear predictions, which is in contrast to the $Z+b$ -jet production. To explain the reason of the observed underestimation, let us consider the relevant differential cross sections as functions of longitudinal momentum fractions and transverse momenta of incoming partons. We show these cross-sections on Figs. 5 and 6.

⁷The uncertainties, connected with the determination of PB TMD parameters are typically much less, than the estimated scale uncertainties and are not taken into account in this work.

As one can see, the $W + c$ -jet production is dominated by smaller x and broader k_T regions in comparison with the $Z + b$ -jet production case. The corresponding off-shell production amplitudes are known to be suppressed in the large k_T domain [43]. We demonstrate this effect in Fig. 7 (left), where the ratios of the reduced cross sections of (18) and (19) calculated with off-shell and on-shell production amplitudes are presented. We find that at $k_T \sim 20$ GeV the off-shell amplitude becomes greatly suppressed. However, a large part of the $W + c$ events comes from the region of $k_T \sim 20$ GeV, as one can see from Fig. 6. Since the considered TMD parton densities were fitted with on-shell matrix elements (see [19, 26]), the suppression results in the drop of the total cross section, thus leading to the observed underestimation. The observed flat behavior at relatively low k_T is connected with the kinematical cuts applied in the CMS analysis [24]. To investigate it in more details we repeat the calculations with different cuts on the transverse momentum of the produced c -quark without any other restrictions on the phase space. One can see, that with increasing the p_T^{cut} the plateau continues until a larger value of $k_T \sim p_T^{\text{cut}}$. In the case of a small value of p_T^{cut} we obtain a steep behaviour starting from practically zero k_T . A similar observation was made in [43] for charm and beauty quark photoproduction at HERA, where the heavy quark mass played the role of p_T^{cut} . Thus, we conclude that to describe the overall normalization of $W + c$ -jet production [24] the appropriate fit of the parameters of considered TMD parton distributions with proper off-shell treatment of production amplitudes is needed.

Finally, we also make a prediction for the p_T^W -distribution in the $W + c$ production case (Fig. 8). One can see, that the CCFM and PB approaches result in different shapes of the distribution, however, the position of the peak remains the same. Like in the case of $Z + b$ production, the difference in the shapes can be explained by a more accurate treatment of the quark-initiated subprocesses within the PB calculations.

4 Conclusion

We have studied the associated production of Z and W bosons and charm or beauty quark jets at the LHC conditions using the TMD factorization framework. We have applied the TMD parton distributions in a proton obtained from the recent PB method as well as from the CCFM evolution equation. For the PB approach, our prescription merges the $\mathcal{O}(\alpha\alpha_s)$ calculations with several tree-level $\mathcal{O}(\alpha\alpha_s^2)$ off-shell production amplitudes. For the CCFM scenario, our consideration is based on the $\mathcal{O}(\alpha\alpha_s^2)$ off-shell gluon-gluon fusion subprocess $g^*g^* \rightarrow Z^0/W^\pm Q\bar{Q}$ and some subleading $\mathcal{O}(\alpha\alpha_s^2)$ subprocesses involving quark interactions, taken into account in conventional QCD factorization. We have found that the $W + c$ and $Z + b$ cross sections, calculated within the PB and CCFM-based schemes with the proper choice of leading and next-to-leading subprocesses in the k_T -factorization, are in good agreement with each other. Thus we have established a correspondence between these two scenarios. We have demonstrated the necessity for the proper off-shell treatment of the production amplitudes in determination of the parameters of the TMD parton densities in a proton.

Acknowledgements

The authors thank S.P. Baranov for useful discussions on the topic. A.V.L. and M.A.M. are grateful to DESY Directorate for the support in the framework of Cooperation Agreement between MSU and DESY on phenomenology of the LHC processes and TMD parton

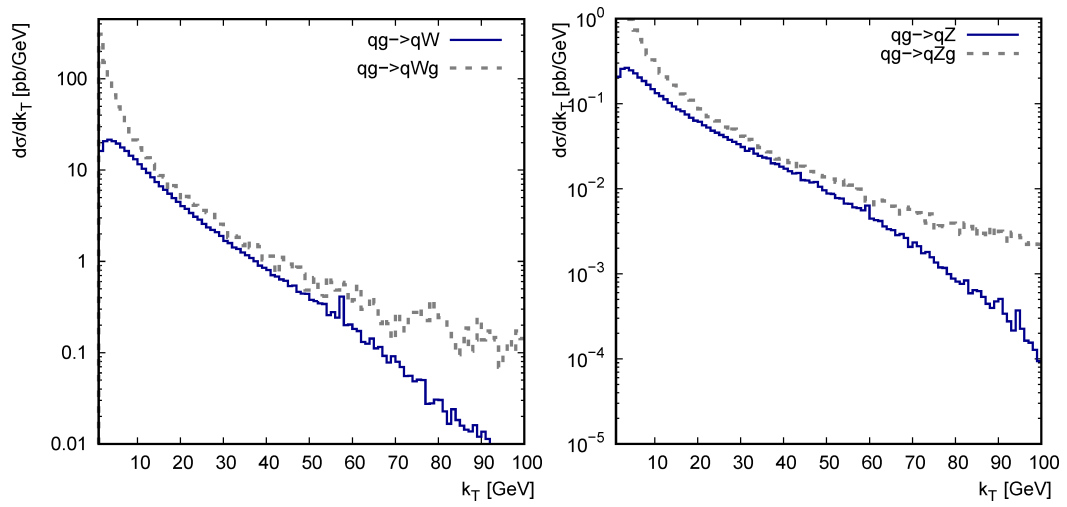


Figure 1: Left panel: distribution for $W^- + c$ production in channel (19) as a function of the transverse momentum of one of the initial partons k_T (solid line) and the same distribution for the subprocess (17) as a function of the transverse momentum of the final gluon p_T (dashed line). Right panel: the same distributions for $Z + b$ production in channels (18) (solid line) and (14) (dashed line).

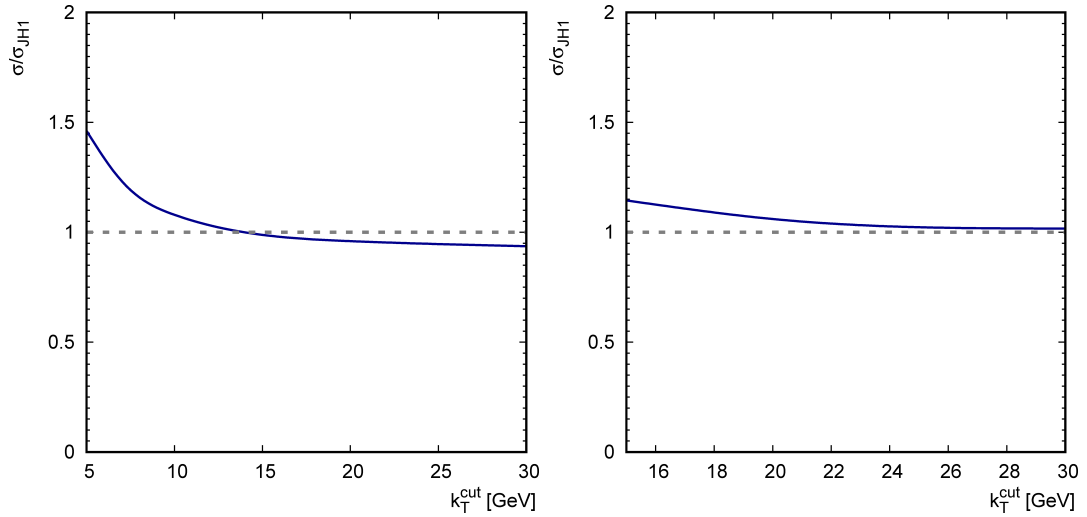


Figure 2: Dependence of the fiducial cross section normalized to the cross section, obtained with JH'2013 set 1 TMD parton densities, as a function of k_T^{cut} . Left panel: $W^- + c$ production. Right panel: $Z + b$ production

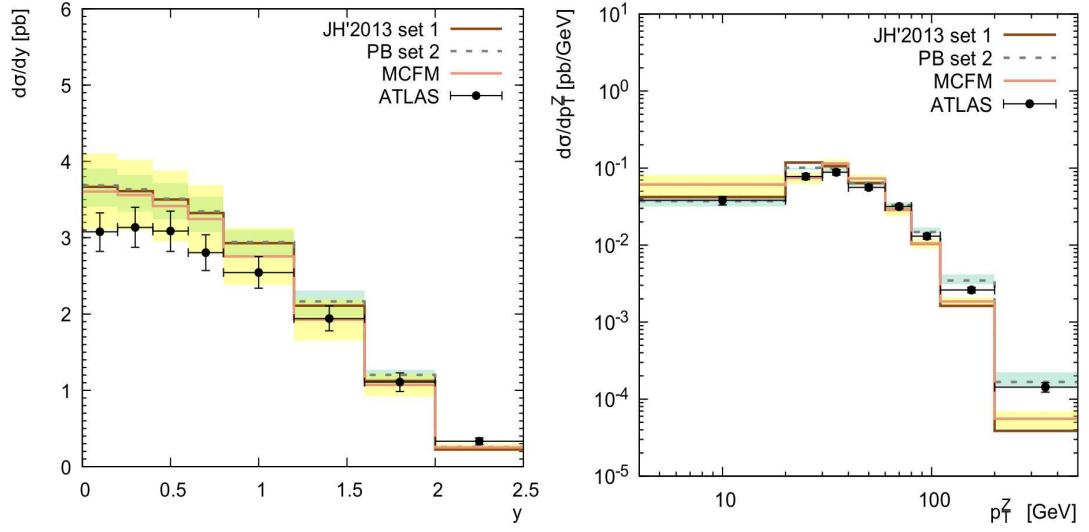


Figure 3: Cross sections of $Z + b$ -production as functions of the Z -boson rapidity (left) and transverse momentum (right). The solid brown line corresponds to the the CCFM approach with JH'2013 set 1 TMD parton density; the grey dashed line corresponds the PB approach with PB-NLO-HERAI+II-2018 set 2 TMD parton densities; the solid pink line corresponds to the collinear factorization approach in NLO. The data are from ATLAS [22].

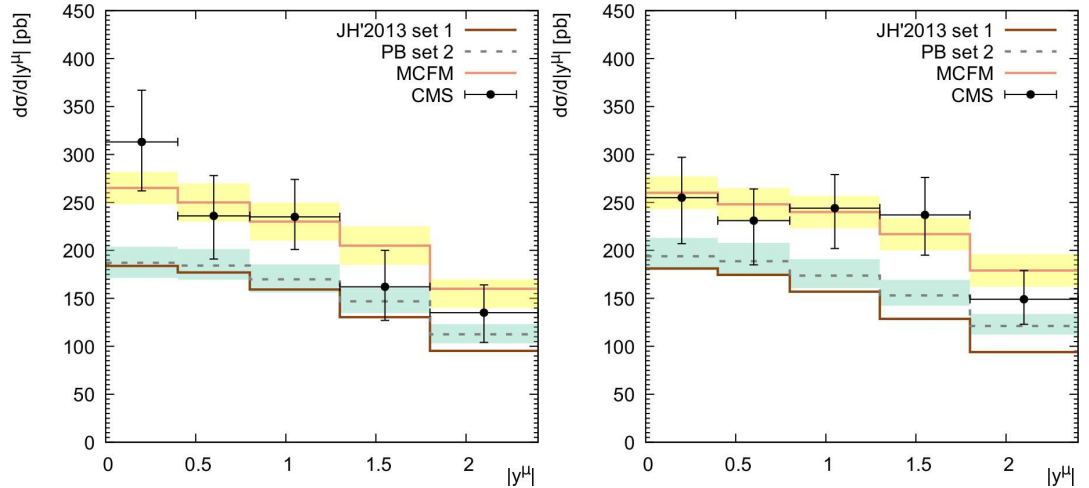


Figure 4: Cross sections of $W + c$ production as functions of the decay muon rapidity. The notations are the same, as on the previous figure. Left panel: $W^+ + \bar{c}$ production case. Right panel: $W^- + c$ production case. The data are from CMS [24].

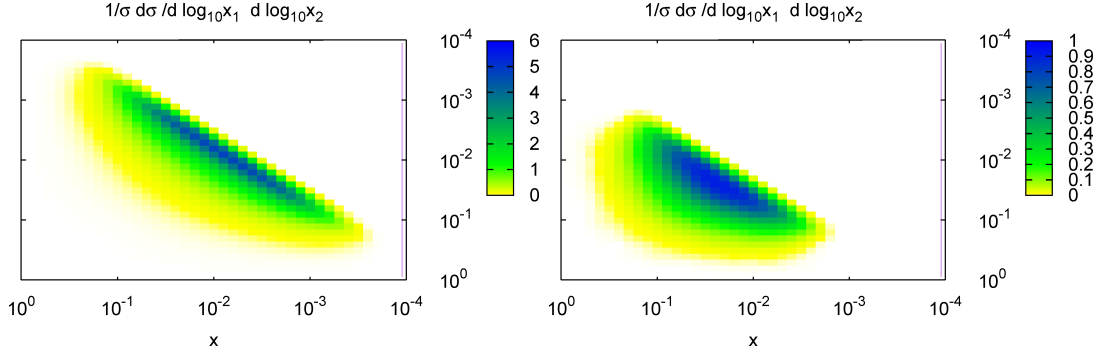


Figure 5: Normalized 2-dimensional cross sections as functions of the initial partons longitudinal momenta fractions x_1 and x_2 . Left panel: $W^- + c$ production case. Right panel: $Z + b$ production case.

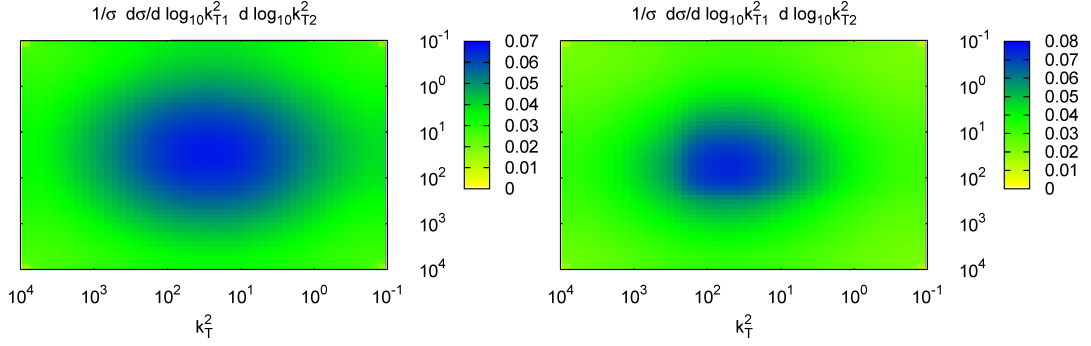


Figure 6: Normalized 2-dimensional cross sections as functions of the initial partons transverse momenta squared k_{T1}^2 and k_{T2}^2 . Left panel: $W^- + c$ production case. Right panel: $Z + b$ production case.

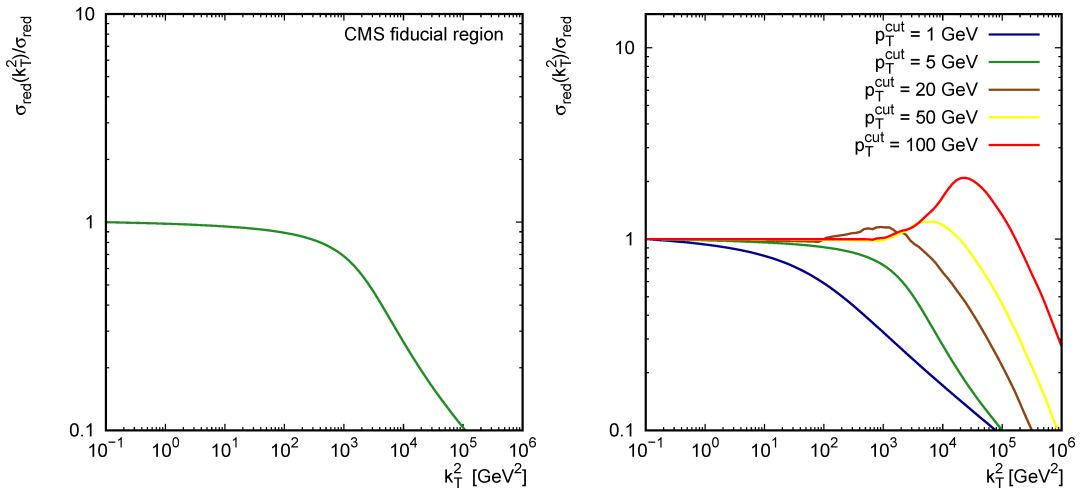


Figure 7: The ratio of 'reduced' cross-sections, calculated with off-shell and on-shell matrix elements for the subprocess (19) (see explanations in the text). Left panel: the ratio in experimental cuts of CMS. Right panel: only cuts on p_T^c is kept in the range from 1 to 100 GeV.

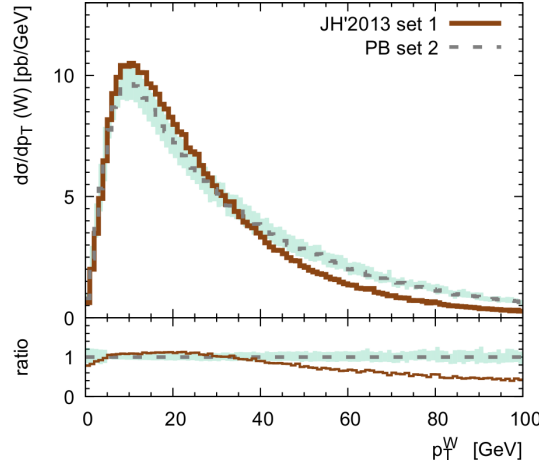


Figure 8: Cross sections of $W^- + c$ production as functions of the W -boson transverse momentum. The notations are the same, as on the previous figure.

densities. M.A.M. was also supported by a grant of the foundation for the advancement of theoretical physics and mathematics "Basis" 17-14-455-1.

References

- [1] R. Angeles-Martinez et al., Acta Phys. Polon. B **46**, 2501 (2015).
- [2] L.V. Gribov, E.M. Levin, M.G. Ryskin, Phys. Rep. **100**, 1 (1983);
E.M. Levin, M.G. Ryskin, Yu.M. Shabelsky, A.G. Shuvaev, Sov. J. Nucl. Phys. **53**, 657 (1991).
- [3] S. Catani, M. Ciafaloni, F. Hautmann, Nucl. Phys. B **366**, 135 (1991);
J.C. Collins, R.K. Ellis, Nucl. Phys. B **360**, 3 (1991).
- [4] E.A. Kuraev, L.N. Lipatov, V.S. Fadin, Sov. Phys. JETP **44**, 443 (1976);
E.A. Kuraev, L.N. Lipatov, V.S. Fadin, Sov. Phys. JETP **45**, 199 (1977);
I.I. Balitsky, L.N. Lipatov, Sov. J. Nucl. Phys. **28**, 822 (1978).
- [5] M. Ciafaloni, Nucl. Phys. B **296**, 49 (1988);
S. Catani, F. Fiorani, G. Marchesini, Phys. Lett. B **234**, 339 (1990);
S. Catani, F. Fiorani, G. Marchesini, Nucl. Phys. B **336**, 18 (1990);
G. Marchesini, Nucl. Phys. B **445**, 49 (1995).
- [6] V.N. Gribov, L.N. Lipatov, Sov. J. Nucl. Phys. **15**, 438 (1972);
L.N. Lipatov, Sov. J. Nucl. Phys. **20**, 94 (1975);
G. Altarelli, G. Parisi, Nucl. Phys. B **126**, 298 (1977);
Yu.L. Dokshitzer, Sov. Phys. JETP **46**, 641 (1977).
- [7] M.A. Kimber, A.D. Martin, M.G. Ryskin, Phys. Rev. D **63**, 114027 (2001);
A.D. Martin, M.G. Ryskin, G. Watt, Eur. Phys. J. C **31**, 73 (2003).
- [8] F. Hautmann, H. Jung, A. Lelek, V. Radescu, R. Zlebcik, Phys. Lett. B **772**, 446 (2017).
- [9] F. Hautmann, H. Jung, A. Lelek, V. Radescu, R. Zlebcik, JHEP **1801**, 070 (2018).

- [10] A.D. Martin, M.G. Ryskin, G. Watt, Eur. Phys. J. C **66**, 163 (2010).
- [11] A.V. Lipatov, M.A. Malyshev, H. Jung, Phys. Rev. D **100**, 034028 (2019)..
- [12] S.P. Baranov, A.V. Lipatov, arXiv:1906.07182 [hep-ph].
- [13] S.P. Baranov, A.V. Lipatov, M.A. Malyshev, Eur. Phys. J. C **78**, 820 (2018).
- [14] S.P. Baranov, A.V. Lipatov, Phys. Lett. B **785**, 338 (2018).
- [15] N.A. Abdulov, A.V. Lipatov, M.A. Malyshev, Phys. Rev. D **97**, 054017 (2018).
- [16] S.P. Baranov, H. Jung, A.V. Lipatov, M.A. Malyshev, Eur. Phys. J. C **77**, 772 (2017).
- [17] S. Dooling, F. Hautmann, H. Jung, Phys. Lett. B **736**, 293 (2014).
- [18] A. Bermudez Martinez, P. Connor, D. Dominguez Damiani, L.I. Estevez Banos, F. Hautmann, H. Jung, J. Lidrych, M. Schmitz, S. Taheri Monfared, Q. Wang, R. Zlebcik, arXiv:1906.00919 [hep-ph].
- [19] A. Bermudez Martinez, P. Connor, F. Hautmann, H. Jung, A. Lelek, V. Radescu, R. Zlebcik, Phys. Rev. D **99**, 074008 (2019).
- [20] R. Maciula, A. Szczurek, Phys. Rev. D **100**, 054001 (2019).
- [21] F. Hautmann, L. Keersmaekers, A. Lelek, A.M. van Kampen, arXiv:1908.08524 [hep-ph].
- [22] ATLAS Collaboration, JHEP **1410**, 141 (2014).
- [23] CMS Collaboration, JHEP **12**, 039 (2013).
- [24] CMS Collaboration, Eur. Phys. J. C **79**, 269 (2019).
- [25] M. Deak, F. Hautmann, H. Jung, K. Kutak, DESY-10-179; arXiv:1012.6037 [hep-ph].
- [26] F. Hautmann, H. Jung, Nucl. Phys. B **883**, 1 (2014).
- [27] F. Hautmann, M. Hentschinski, H. Jung, Nucl. Phys. B **865**, 54 (2012).
- [28] N.A. Abdulov, H. Jung, A.V. Lipatov, G.I. Lykasov, M.A. Malyshev, Phys. Rev. D **98**, 054010 (2018).
- [29] F. Hautmann, H. Jung, S. Taheri Monfared, Eur. Phys. J. C **74**, 3082 (2014).
- [30] S. Taheri Monfared, F. Hautmann, H. Jung, M. Schmitz, PoS **DIS2019**, 136 (2019).
- [31] S.P. Baranov, A.V. Lipatov, N.P. Zotov, Phys. Rev. D **78**, 014025 (2008).
- [32] M. Deak, F. Schwennsen, JHEP **09**, 035 (2008).
- [33] H. Jung, S.P. Baranov, M. Deak, A. Grebenyuk, F. Hautmann, M. Hentschinski, A. Knutsson, M. Kramer, K. Kutak, A.V. Lipatov, N.P. Zotov, Eur. Phys. J. C **70**, 1237 (2010).
- [34] S.P. Baranov, A.V. Lipatov, M.A. Malyshev, in preparation.

- [35] L.N. Lipatov, M.I. Vyazovsky, Nucl. Phys. B **597**, 399 (2001);
A.V. Bogdan, V.S. Fadin, Nucl. Phys. B **740**, 36 (2006);
M. Hentschinski, A. Sabio Vera, Phys. Rev. D **85**, 056006 (2012);
M. Hentschinski, Nucl. Phys. B **859**, 129 (2012).
- [36] A. van Hameren, JHEP **1407**, 138 (2014).
- [37] A. van Hameren, K. Kutak, T. Salwa, Phys. Lett. B **727**, 226 (2013).
- [38] A. van Hameren, Comput. Phys. Commun. **224**, 371 (2018).
- [39] <http://tmd.hepforge.org>
- [40] L.A. Harland-Lang, A.D. Martin, P. Motylinsky, R.S. Thorne, Eur. Phys. J. C **75**, 204 (2015).
- [41] Particle Data Group, Chin. Phys. C **40**, 100001 (2016).
- [42] J.M. Campbell, R.K. Ellis, Phys. Rev. D **60**, 113006 (1999);
J.M. Campbell, R.K. Ellis, Nucl. Phys. Proc. Suppl. **205—206**, 10 (2010);
J.M. Campbell, R.K. Ellis, J. Phys. G **42**, 015005 (2015).
- [43] S.P. Baranov, H. Jung, L. Jönsson, S. Padhi, N.P. Zotov, Eur. Phys. J. **C24**, 425 (2002).